Self-diffusion mechanism in solid sodium by NMR

G. Brünger and O. Kanert
Institut für Physik, Universität Dortmund, West Germany

D. Wolf
Argonne National Laboratory, Argonne, Illinois 60439

(Received 3 March 1980)

The self-diffusion mechanism in solid sodium has been determined by means of NMR. For that purpose, the spin-lattice relaxation times T_1 and $T_{1\rho}$ and the Knight shift K of ^{23}Na in ultrapure sodium have been measured as a function of temperature in the range of $10 \leq T \leq 371$ K (melting point). At all temperatures, the Zeeman relaxation time T_1 is determined by conduction electrons leading to a volume-corrected Korringa relation of $T_1 T = 4.68 \pm 0.13$ K s. In the temperature range 150–280 K, an additional contribution to the rotating-frame relaxation rate, $T_{1\rho}^{-1}$, arising from fluctuations in the nuclear dipole interaction due to atomic self-diffusion is observed. By comparing the motion-induced part of the relaxation rate with the tracer measurements of Mundy, the correlation factor and thus the self-diffusion mechanism in sodium is determined. The following three diffusion mechanisms have been assumed to interpret the observed curvature in the Arrhenius plot: (1) a combination of mono- and divacancies; (2) monovacancies alone with a temperature-dependent pre-exponential factor and activation enthalpy; and (3) monovacancies with the possibility of vacancy double jumps. It is found that the temperature dependence of the measured correlation factor is consistent with the simultaneous migration of mono- and divacancies while the other two mechanisms can be ruled out as solely responsible for the observed effects.

I. INTRODUCTION

Characteristic of the self-diffusion in many face-centered-cubic (fcc) and body-centered-cubic (bcc) metals is the curvature in the observed Arrhenius plot of the tracer self-diffusion coefficient D^T. While the relatively small deviations from Arrhenius behavior observed in fcc metals are usually attributed to the formation and migration of divacancies at higher temperatures, the question as to the microscopic origin of the rather pronounced curvatures observed in bcc metals is still rather controversial. In past years essentially three explanations for this phenomenon have been offered:

(1) Seeger and Mehrer[1] and Mehrer[2,3] have interpreted the curvature in terms of the simultaneous migration of mono- and divacancies with only a minor contribution arising from the temperature dependence of the activation energy via the so-called α term (SM model). If this term is neglected the temperature dependence of D^T may be written as follows[1–3]:

$$D^T = D_{01}^T e^{-E_{1V}/kT} + D_{02}^T e^{-E_{2V}/kT} , \quad (1)$$

where the four parameters $D_{0\alpha}^T$ and $E_{\alpha V}$ ($\alpha = 1, 2$) are the temperature-independent pre-exponential factors and activation enthalpies, respectively, associated with mono- and divacancies, and k denotes the Boltzmann factor.

(2) According to Gilder and Lazarus[4] the curvatures observed in most bcc metals may equally well be explained in terms of the thermal expansion of highly relaxed monovacancies (GL model). The curvature is then attributed to the temperature dependence of D_{01}^T and E_{1V} which may be characterized[4] by a single parameter μ_v. Hence, in the GL model the Arrhenius plot is governed by only three parameters, according to[4]

$$D^T = d_0^T e^{-q_0/kT} e^{\mu_V T/2k} , \quad (2)$$

where d_0^T and q_0 denote the pre-exponential factor and the activation enthalpy for monovacancy migration at some reference temperature which is larger than the Debye temperature. In support of this model Varatsos, Ludwig, and Falter[5] have interpreted the pressure dependence of D^T in sodium[6] in terms of the compressibility of monovacancies alone.

(3) From their molecular dynamics computer simulations Bennett[7] and Da Fano and Jaccucci[8] concluded that the curvature in the Arrhenius plot of sodium arises from nearest-neighbor ($\langle 111 \rangle$) double jumps of monovacancies (FJ model). They claim that at the melting point about 25% of all vacancy jumps are such double jumps.

In recent years the self-diffusion properties of solid sodium have been investigated rather thoroughly. The radio-tracer self-diffusion coefficient, D^T, as well as its pressure and mass dependence were measured by Mundy *et al.*[9] and Mundy.[6] Feder and Charbnau[10] and Adlhart, Fritsch, and Lüscher[11] have presented simultaneous measurements of the thermal expansion and of the lattice parameter from which they conclude that the dominant thermal-equilibrium defects are vacancies. Together with Mundy's observation[6] of an increase of the activation volume and a decrease of the isotope effect with increasing temperature, one would tend to conclude that the Seeger-Mehrer model properly describes the origin of the observed curvature in the Arrhenius plot.

Peterson[12] has recently reviewed the evidence for each of the above mechanisms. He concludes that mechanisms (2) and (3) may be consistent with the observed curvature of the Arrhenius plot but point-defect data other than tracer diffusion requires two types of defect for all metals where such data is available.

Recent theoretical progress in the extraction of correlation times for point-defect diffusion mechanisms for NMR,[13–15] quasielastic neutron scattering,[16] and Mössbauer line broadening experiments[17] has substantially increased the accuracy with which the macroscopic self-diffusion constant, D^{SD}, may be determined by means of these nontracer techniques. As proposed recently in a quantitative manner,[18,19] the measurement of D^{SD} by one of these methods and the subsequent comparison with D^T values, i.e., the determination of the correlation factor

$$f = D^T/D^{SD} \quad , \tag{3}$$

should enable one to investigate which of three mechanisms outlined above is mainly responsible for the curvature of the Arrhenius plot.

Two attempts along these lines have been made very recently. In the case of solid lithium, Messer[20,21] has shown that the combination of mono- and divacancies permits a self-consistent interpretation of his NMR results and the radio-tracer data of Lodding *et al.*[22] However, other sources for the curvature such as mechanisms (2) and (3) outlined above which might also permit a self-consistent interpretation have not been considered yet.

Ait-Salem *et al.*[23] and Göltz *et al.*[24] have studied the quasielastic line broadening in solid sodium at temperatures just below the melting point. Their comparison with Mundy's radiotracer data[6] strongly suggests that mechanisms (2) and (3) may be ruled out as solely responsible for the observed curvature in the Arrhenius plot and that divacancies consisting of monovacancies in first, second, and fourth nearest-neighbor configurations are the cause for the observed curvature in the Arrhenius plot.

Similar to Messer's work,[20] we have performed nuclear-spin-relaxation experiments to elucidate the origin of the curvature in the Arrhenius plot of solid sodium. For that purpose we have measured the temperature dependence of spin-lattice relaxation time, $T_{1\rho}$, in the rotating frame. Earlier Holcomb and Norberg[25] reported measurements of the spin-lattice relaxation time, T_1, and the spin-spin relaxation time T_2. From the latter an estimate was obtained for the activation energy associated with sodium self-diffusion. By investigating the pressure dependence of T_2, Hultsch and Barnes[26] obtained an estimate for the activation volume of the point defect responsible for self-diffusion in sodium.

II. EXPERIMENTAL DETAILS

The nuclear-spin-relaxation measurements were carried out on ultrapure polycrystalline sodium samples. To avoid skin effect distortions of the NMR signal, the samples consisted of small sodium spheres with an average particle size of about 10 μm embedded in paraffin wax. The samples were prepared in two different ways:

(i) Ultrapure sodium (99.95%) supplied by three different companies (Alfa Metals, Kawecki, and Baker) together with an amount of paraffin wax was heated to a temperature of 150 °C in a large glove box with an extremely pure He atmosphere (impurity ≤ 10 ppm). The melt was dispersed by ultrasonic agitation forming a sort of emulsion consisting of sodium droplets surrounded by paraffin wax. The emulsion was transferred into sample ampules, which were sealed off, cooled down to room temperature, and solidified. The volume of the samples was about 0.3 to 0.8 cm^3 with a concentration of sodium of about 30 to 40%.

(ii) A part of the sodium-paraffin wax melt was filled into a stainless-steel vessel and whipped to form a dispersion by joggling the melt together with two stainless-steel spheres of 7 mm diameter at a frequency of about 30 Hz. The procedure was carried out under air pressure. As described above, the emulsion was then poured into glass tubes and cooled down at room temperature.

Within the experimental error, both types of samples lead to the same experimental results for the Knight-shift measurements as well as for all nuclear-spin-relaxation measurements. This indicates that the influence of surface impurities and bulk impurities on the NMR data is negligible.

The nuclear magnetic resonance of ^{23}Na was observed with a Bruker SXP 4-100 coherent pulsed NMR spectrometer including an on-line computer system (Data Lab DL 905 and Varian 620 1) to improve the signal-to-noise ratio by signal averaging and to evaluate the experimental data. The measurements were made at magnetic fields of 1.45 and 4.25

T corresponding to Larmor frequencies of 16.4 and 47.9 MHz, respectively.

The sample was mounted inside a Leybold variable-temperature He-evaporation cryostat. Temperatures were stabilized with a temperature-regulation system within ± 0.2 K over the temperature range investigated (10 to 371 K). Sample temperatures were measured with a Au-Fe versus Cr-Ni thermocouple, which were calibrated against liquid nitrogen. The overall accuracy of the temperature determination was ± 0.5 K.

Knight shifts were measured by comparing the beat frequency of the free induction decay of ^{23}Na in sodium following a $\frac{1}{2}\pi$ pulse with the beat frequency of ^{23}Na of solid NaCl. The width of a $\frac{1}{2}\pi$ pulse was about 4 μs corresponding to a H_1 field of about 50 G. The overall dead time of the spectrometer of about 7 μs was small compared to the width of the ^{23}Na free-induction decay, which was 120 μs at low temperatures.

Spin-lattice relaxation times T_1 were measured with π-$\frac{1}{2}\pi$ pulse sequences, whereas the spin-lattice relaxation times in the rotating frame, $T_{1\rho}$, were determined with the spin-locking technique (consisting of an intense $\frac{1}{2}\pi$ pulse followed by a long pulse of strength H_1 shifted in rf phase by $\frac{1}{2}\pi$ with respect to the first pulse). The locking field H_1 was calibrated by measuring the voltage induced by H_1 in a small output coil close to the sample relative to the induction voltage of the $\frac{1}{2}\pi$ pulse. The pulse sequence used to measure the rotating-frame relaxation time in zero H_1 field, T_{1D}, was that suggested by Jeener and Broeckaert.[27] First, Zeeman order is transferred to the dipolar system by applying a $\pi/2|_x - T_2 - \pi/4|_y$ pulse pair. The system is then allowed to relax during a time τ. At time τ, a $\pi/4$ reading pulse is applied to measure the magnitude of the remaining magnetization.

Relaxation times were determined with an accuracy of about $\pm 3\%$ for relaxation fields H_0 and H_1 which were large compared to the local field H_L, and with an accuracy of about $\pm 10\%$ for $H_1 \lesssim H_L$.

III. EXPERIMENTAL RESULTS AND INTERPRETATION

A. Experimental results

^{23}Na spin-lattice relaxation times T_1 and $T_{1\rho}$ were measured at various values of the relaxation field in solid sodium from 10 K to the melting point (371 K).

A logarithmic plot of the experimental T_1 and $T_{1\rho}$ data versus reciprocal temperature is shown in Fig. 1. The figure also includes some T_{1D} data obtained in the temperature region between 80 and 180 K. As mentioned above, neither the spin-lattice relaxation time T_1 nor the spin-lattice relaxation time in the rotating frame, $T_{1\rho}$, depends on the sample preparation.

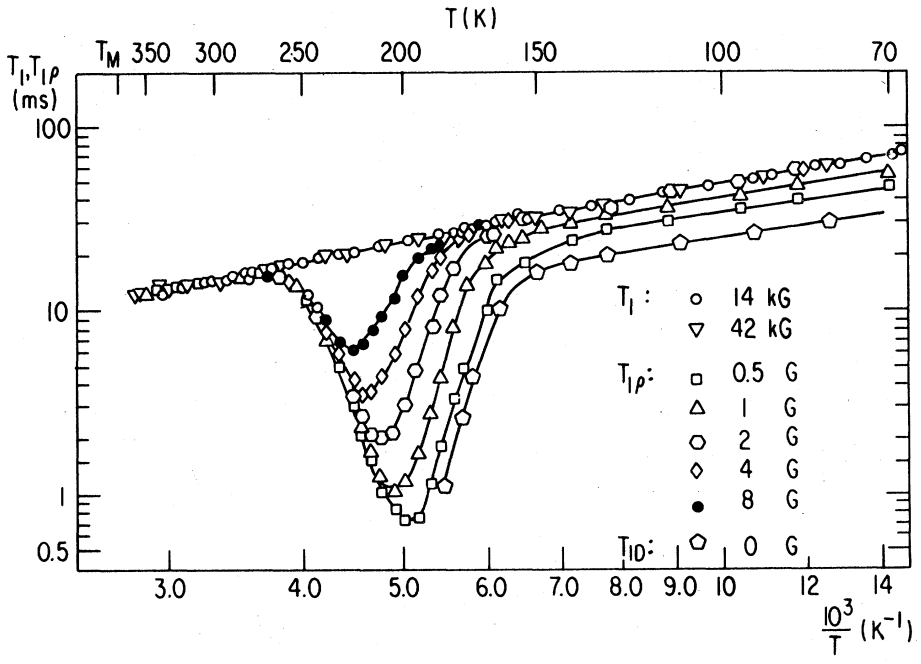

FIG. 1. Temperature dependence of the ^{23}Na spin-lattice relaxation times T_1, $T_{1\rho}$, and T_{1D} in powdered samples of solid sodium for different relaxation fields.

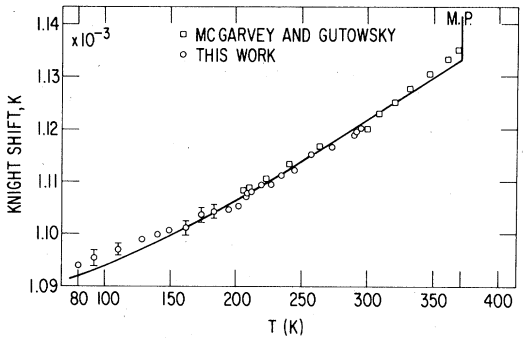

FIG. 2. Knight shift K of ^{23}Na in solid sodium as a function of temperature. The squares are the results of McGarvey and Gutowsky (Ref. 29). Only a few typical error bars are shown.

This ensures that a measurable influence of impurities in the sample on the relaxation behavior does not exist.

Obviously, in the entire temperature region the Zeeman relaxation time T_1 is due to a single relaxation mechanism, namely the Korringa mechanism. In contrast the relaxation time in the rotating frame, $T_{1\rho}$, consists of two different contributions. The field-dependent minima of $T_{1\rho}$ in Fig. 1 are due to diffusive jumps of Na atoms. In the minima region, this relaxation contribution dominates over the $T_{1\rho}$ contribution due to conduction electrons.

In order to study the Korringa process for solid sodium in more detail, the ^{23}Na Knight shift was measured from 80 K to the melting point. The results are shown in Fig. 2. The observed values agree quite well with earlier results of McGarvey and Gutowsky[28] which have also been plotted in Fig. 2.

B. Conduction-electron properties

The principal contribution to the measured Knight shift K in nonmagnetic (simple) metals is usually due to the hyperfine field of the polarized s-like conduction electrons interacting with the nucleus via the Fermi-contact interaction. This contribution to K is given by[29]

$$K = \frac{8}{3}\pi\gamma_e^2\hbar^2\langle|\psi(0)|^2\rangle_{E_F}\rho(E_F) \ , \qquad (4)$$

where γ_e is the electron gyromagnetic ratio. $\langle|\psi(0)|^2\rangle_{E_F}$ denotes the average density of s-like Fermi-surface electrons at the nucleus, and $\rho(E)$ symbolizes the electronic density of states. Although Eq. (4) contains no explicit temperature dependence, K may exhibit a weak temperature dependence due to the effects of thermal expansion[28] and to intrinsic temperature effects produced by electron-phonon interactions.[30]

Assuming $\langle|\psi(0)|^2\rangle_{E_F}$ to be independent of temperature, for a nearly free-electron gas the temperature dependence of the Knight shift K should follow the relation $\rho(E_F) \propto V^{2/3}$ which leads to the expression[28]

$$K(T) = K(300\ \mathrm{K})[V(T)/V(300\ \mathrm{K})]^{2/3} \ , \qquad (5)$$

where V denotes the sample volume. Using the thermal-expansion coefficient for solid sodium[31] enables us to compare Eq. (5) with our experimental data. The result is shown in Fig. 2. The solid line calculated from Eq. (5) and the experimental Knight-shift data agree quite well. This confirms the s-like character of conduction electrons in sodium.

Similar to the Knight shift, spin-lattice relaxation in simple metals is also dominated by the magnetic Fermi-contact hyperfine interaction. The corresponding relaxation time $(T_1)_e$ is related to the Knight shift K by the Korringa relation[31]

$$(T_1)_e TK^2 = \frac{\hbar\Delta}{4\pi k}\left(\frac{\gamma_e}{\gamma_N}\right)^2 \ , \qquad (6)$$

where γ_N is the nuclear gyromagnetic ratio, while Δ is a factor of order unity introduced to account for effects of conduction-electron correlation.[32] Together with Eq. (5) one expects for the temperature dependence of $(T_1)_e T$

$$(T_1)_e T = (\mathrm{const})[V(300\ \mathrm{K})/V(T)]^{4/3} \ . \qquad (7)$$

In Fig. 3 the experimental T_1 values corrected by the volume factor $[V(T)/V(300\ \mathrm{K})]^{4/3}$ have been plotted versus reciprocal temperature. The slope of the straight line in Fig. 3 is represented by $T_1 T = 4.68 \pm 0.13$ K s. Figure 3 demonstrates that in the entire temperature region the magnetic contact hyperfine interaction is indeed the dominant Zeeman relaxation mechanism. The value for $T_1 T$ given above

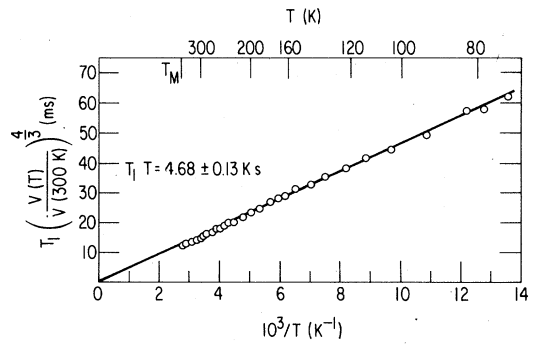

FIG. 3. Volume-corrected relaxation time T_1 for ^{23}Na in solid sodium as a function of reciprocal temperature. The straight line confirms a Korringa mechanism as the source of the Zeeman relaxation in the entire temperature region.

agrees quite well with previous measurements of Holcomb and Norberg[25] who found $T_1T = 4.77 \pm 0.2$ K s. But, contrary to the results of Holcomb and Norberg, who reported a weak (10%) decrease of T_1 with decreasing Larmor frequency (from 9 to 3 MHz), within experimental error our values of T_1 are field independent as is to be expected for *s*-like conduction electrons.

A field dependence of spin-lattice relaxation due to conduction electrons is expected only for relaxation fields comparable to the local field. In the case of $T_{1\rho}$, this field dependence is expected to follow the relationship[29,33]

$$(T_{1\rho})_e = (T_1)_e \frac{H_1^2 + H_{D\rho}^2}{H_1^2 + \delta H_{D\rho}^2} \quad . \tag{8}$$

Here $H_{D\rho}$ denotes the local field in the rotating frame. According to Wolf,[33] the field-independent factor δ in Eq. (8) should equal $\delta = 1 + \sqrt{3}/2 \approx 1.87$ while according to Hebel and Slichter[29] δ should equal $\delta = 2$. Figure 4 shows the $(T_{1\rho})_e$ values extracted from the results in Fig. 1 for different values of the rotating field H_1. The fit of Eq. (8) (solid line) to these values yields the best-fit parameters $H_{D\rho} = 0.50 \pm 0.05$ G and $\delta = 2.0 \pm 0.1$.

The value of $H_{D\rho}$ is in good agreement with the value $H_{D\rho} = 0.46$ G calculated via the dipolar second moment.[34] To the extent of our knowledge, our value of δ is among the lowest obtained for any metal. According to Wolf,[33] even a relatively small number of electric-field-gradient sources (associated, e.g., with dislocations or impurities which locally destroy the cubic symmetry) should give rise to a marked increase in δ from its limiting (dipolar) value given above, without noticeably increasing the dipolar local field. Since our powdered samples probably contain large amounts of dislocations, it appears difficult to decide whether our best-fit value of δ favors Hebel and Slichter's or Wolf's prediction.

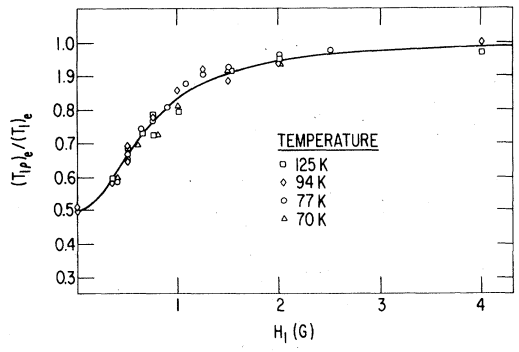

FIG. 4. Field dependence of the electronic contribution to $T_{1\rho}$ for different temperatures. The solid line is obtained from Eq. (8) with the best-fit parameters $\delta = 2.0 \pm 0.1$ and $H_{D\rho} = 0.5 \pm 0.05$ G.

C. Diffusion-induced relaxation contribution

As discussed in connection with Fig. 1, for temperatures between about 160 and 270 K, $T_{1\rho}$ is dominated by self-diffusion of sodium atoms. Figure 5 shows the corresponding relaxation rates which were obtained from Fig. 1 by subtracting the electronic contribution to $T_{1\rho}$, according to

$$\left(\frac{1}{T_{1\rho}}\right)_d = \frac{1}{T_{1\rho}} - \left(\frac{1}{T_{1\rho}}\right)_e \quad . \tag{9}$$

$(1/T_{1\rho})_d$ is due to diffusion-induced fluctuations of dipolar interactions. The dipolar relaxation contribution arising from monovacancies and several modes of divacancy migration in the bcc lattice described by Mehrer[35] was calculated by Wolf.[15] According to this theory, the total dipolar relaxation rate associated with the simultaneous migration of mono- and divacancies may be decomposed as follows:

$$\left(\frac{1}{T_{1\rho}}\right)_d = p_1(T)\left(\frac{1}{T_{1\rho}}\right)_{1V} + p_2(T)\left(\frac{1}{T_{1\rho}}\right)_{2V} \quad , \tag{10}$$

where $p_1(T)$ and $p_2(T)$ denote the probabilities that the jump of an atom is induced by a mono- or divacancy, respectively. $(T_{1\rho}^{-1})_{1V}$ and $(T_{1\rho}^{-1})_{2V}$ are the relaxation rates in the limit in which self-diffusion is solely due to mono- or divacancies, respectively.

In the case of the simultaneous migration of mono- and divacancies in bcc lattices, the probabilities[36] $p_\alpha = D_\alpha/(D_1 + D_2)$ can be written as follows[2,15]:

$$p_1(T) = \frac{1}{1 + D_{21}\exp(-\epsilon E_{1V}/kT)} \tag{11a}$$

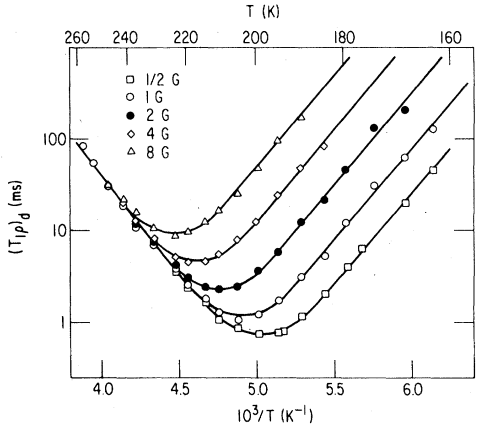

FIG. 5. Diffusion-induced contribution to the relaxation time $T_{1\rho}$ of ^{23}Na in solid sodium vs inverse temperature as obtained from Fig. 1 and Eq. (9). The solid lines are computer fits based on the best-fit parameters presented in Table II (for further details see text).

and

$$p_2(T) = 1 - p_1(T) \ , \tag{11b}$$

where $D_{21} = D_{02}^{SD}/D_{01}^{SD}$ is the ratio of the uncorrelated pre-exponential factors given by Eqs. (1) and (3) while $\epsilon = (E_{2V} - E_{1V})/E_{1V}$. Numerical values for these relaxation rates for both single crystals and powdered bcc and fcc samples have been presented by Wolf[15] in the high-field limit in which the amplitude H_1 of the rotating field is much larger than the dipolar local field in the rotating-frame, $H_{D\rho}$($H_1 >> H_{D\rho}$). This limit is commonly referred to as the "weak-collision" region.[33,37]

To allow for the possibility that divacancies may contribute to the relaxation behavior even at temperatures well below the $T_{1\rho}$ minimum in Fig. 5, $(T_{1\rho}^{-1})_{2V}$ has been calculated in the "strong-collision" limit[37] in which the thermal mixing time T_m is much shorter than the mean time between successive encounters, τ_{enc}($T_m << \tau_{enc}$).[33] According to Slichter and Ailion[37] and Wolf,[14] in this regime $T_{1\rho}^{-1}$ due to point-defect migration is governed by the expression

$$\left(\frac{1}{T_{1\rho}}\right)_d = \frac{H_{D\rho}^2}{H_1^2 + H_{D\rho}^2} \frac{2(a-p)}{\tau} \ , \tag{12}$$

where τ denotes the mean time between successive jumps of an atom. The factor $(a-p)$ usually depends on the orientation of the magnetic Zeeman field, $\vec{H}_0$, with respect to the principal crystal axes.[37,38,14,33] In cubic crystals this anisotropy may be written in terms of the "anisotropy function" $f(\theta, \phi)$ defined by[13,14]

$$f(\theta, \phi) = \sin^2 2\theta + \sin^4\theta \sin^2 2\phi \ , \tag{13}$$

where θ and ϕ characterize the crystallographic orientation of $\vec{H}_0$ (see, e.g., Refs. 13 and 14).

Originally,[37,38] for point-defect diffusion mechanisms the "strong-collision" limit was defined by $T_m << \tau_v$, i.e., thermal mixing was assumed to occur not only between successive encounters but even between successive defect jumps (τ_v denotes the mean time between such jumps). In reality, this condition has not been realized experimentally. Instead, one usually finds that $\tau_v << T_m << \tau_{enc}$. As discussed by Wolf,[14] Eq. (12) is formally correct in both regimes, with different values and anisotropies of $(a-p)$, however.

The results of our calculations for divacancies in fcc and bcc lattices in the regime in which $\tau_v << T_m << \tau_{enc}$ are listed in Table I. For completeness, the results for monovacancies in this region[14] and for both mono-[38] and divacancies[39] in the region in which $T_m << \tau_v$ are also shown. As discussed earlier,[13-15] powder values are obtained by choosing $f(\theta, \phi) = \frac{4}{5}$.

The so-called $1N$-$2N$-$1N$ and $1N$-$2N$-$4N$ mechanisms of divacancy migration in the bcc lattice have been considered earlier by Mehrer.[35] In the $1N$-$2N$-$1N$ mechanism the two vacancies which form the divacancy are assumed to occupy alternately nearest-neighbor ($1N$) and second-nearest-neighbor ($2N$) configurations. In the $1N$-$2N$-$4N$ mechanism considered here, divacancies in $2N$ configurations are assumed to jump—in our case with equal probabilities—into $1N$ or $4N$ configurations. (For further details on these mechanisms, see below.)

According to Eq. (12), in the strong-collision region a plot of the diffusion contribution to $T_{1\rho}$ vs H_1^2 will yield a straight line which may be extrapolated to find the x intercept at $H_1^2 = -H_{D\rho}^2$. Figure 6 shows such a plot for $(T_{1\rho})_d$ at $T = 172$ K; the local field thus obtained is $H_{D\rho} = 0.47 \pm 0.3$ G in good agreement with the value obtained in Sec. III B from the field dependence of $(T_{1\rho})_e$. The slope of the straight line in Fig. 6 yields a factor $a - p = 0.28 \pm 0.04$. This value was obtained using a correlation time $\tau(172\ \text{K}) = 3.3 \pm 0.4$ msec based on the mono-divacancy model discussed in detail below. This result does not agree very well with the theoretical value of 0.413 for monovacancies (see Table I). As seen from Table I, a divacancy contribution leads to a decrease of the theoretical value for $(a-p)$ but seems to be unable to explain the total magnitude of the difference between the experimental and theoretical value.

If H_1 is large enough to suppress thermal mixing ($H_1 >> H_{D\rho}$), one has instead of Eq. (12)[14,33]

$$\left(\frac{1}{T_{1\rho}}\right)_d = \frac{\frac{3}{4}H_{D\rho}^2}{H_1^2 + \frac{3}{4}H_{D\rho}^2} \frac{2(a-p)}{\tau} \ . \tag{14}$$

The transition region between weak and strong collisions occurs when T_m and $(T_{1\rho})_d$ are of the same order of magnitude.[33] In practice this requires H_1 and $H_{D\rho}$ to be similar in value.[36] In Fig. 7 this transition is analyzed at the temperature $T = 172$ K (see also Fig. 6). Shown is a doubly-logarithmic plot of $(T_{1\rho})_d$ vs H_1^2 over a wider range of H_1^2 values than shown in Fig. 6. The two solid lines were obtained from Eqs. (12) and (14) with the value of $2(a-p)/\tau$ obtained in connection with Fig. 6. As is seen from Fig. 7, at lower rotating fields, the experimental points represent a rather good fit to the strong-collision curve obtained from Eq. (12) while at higher H_1 values better agreement is obtained with the weak-collision expression.[14,33] According to Fig. 7, the transition occurs roughly in the region in which $1.5H_{D\rho} \lesssim H_1 \lesssim 3H_{D\rho}$.

To extract self-diffusion coefficients from the experimental $(T_{1\rho})_d$ values in Fig. 5, we follow the usual procedure of first determining the mean time, τ, between successive atom jumps and then, calculating the uncorrelated self-diffusion coefficient, D^{SD}, via the Einstein-Smoluchovski relation,

$$D^{SD} = d^2/6\tau \ , \tag{15}$$

TABLE I. Values for $(a\text{-}p)$ in Eq. (12) for relaxation via mono- and divacancies in the fcc and bcc lattices. $2a_0$ denotes the cube edge of the related elementary cell.

Lattice type			Single crystals	Powder average $[f(\theta,\phi)=0.8]$
$(a\text{-}p)$ for $\tau_v \ll T_m \ll \tau_{enc}$ in units of a_0^{-6}	fcc	$1V^a$	$\frac{0.472+0.206f(\theta,\phi)}{1.074+0.459f(\theta,\phi)}$	0.442
		$2V$	$\frac{0.207+0.094f(\theta,\phi)}{1.074+0.459f(\theta,\phi)}$	0.196
		$1V^a$	$\frac{0.091+0.073f(\theta,\phi)}{0.232+0.162f(\theta,\phi)}$	0.413
	bcc	$2V$ $(1N\text{-}2N\text{-}1N)$	$\frac{0.043+0.033f(\theta,\phi)}{0.232+0.162f(\theta,\phi)}$	0.192
		$2V$ $(1N\text{-}2N\text{-}4N)$	$\frac{0.045+0.038f(\theta,\phi)}{0.232+0.162f(\theta,\phi)}$	0.209
$(a\text{-}p)$ for $\tau_v \gg T_m$ in units of a_0^{-6}	fcc	$1V^{b,c}$	$\frac{0.863+0.336f(\theta,\phi)}{1.077+0.460f(\theta,\phi)}$	0.783
		$2V^{d,c}$	$\frac{0.769+0.375f(\theta,\phi)}{1.077+0.460f(\theta,\phi)}$	0.740
	bcc	$1V^{b,c}$	$\frac{0.179+0.110f(\theta,\phi)}{0.233+0.162f(\theta,\phi)}$	0.736
		$2V^{d,c}$ $(1N\text{-}2N\text{-}1N)$	$\frac{0.163+0.100f(\theta,\phi)}{0.233+0.162f(\theta,\phi)}$	0.670

[a]See Ref. 14.
[b]See Ref. 38.
[c]Originally these results were presented in units of $16a_0^{-6}$ and for the special case in which $\phi=0$.
[d]See Ref. 39.

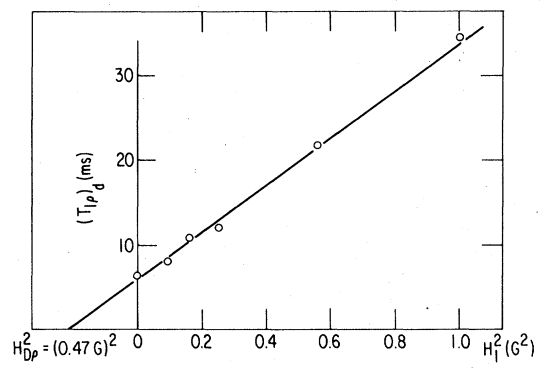

FIG. 6. Plot of the diffusion-induced part of $T_{1\rho}$ vs H_1^2 of ^{23}Na in sodium at 172 K. The plot provides verification of Eq. (12) with the best-fit parameters $a-p=0.28\pm0.04$ and $H_{D\rho}=0.47\pm0.03$ G.

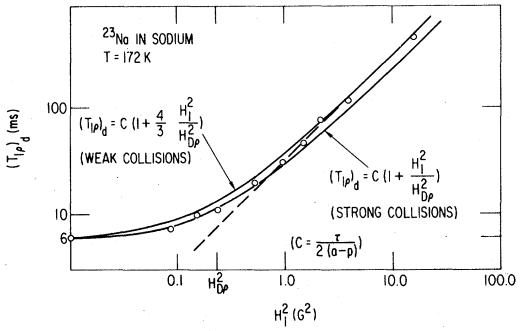

FIG. 7. Doubly-logarithmic plot of $(T_{1\rho})_d$ for ^{23}Na in sodium at 172 K as a function of H_1^2. The solid lines are obtained from Eqs. (12) and (14), respectively. The figure illustrates the transition from the weak-collision region to the strong-collision region in the field range $1.5H_{D\rho} \lesssim H_1 \lesssim 3H_{D\rho}$.

where d is the jump distance.

Thus, for the Gilder-Lazaras (GL) model, in Eq. (10) $p_1(T) \equiv 1$ and, hence, $p_2(T) \equiv 0$ for all temperatures. With the relaxation rates for diffusion via monovacancies presented by Wolf[13–15] it is then, in principle, possible to assign a value of τ to every experimental value of $(T_{1\rho})_d$. This analysis has to take into account, however, the temperature dependence of the pre-exponential factor and the activation energy [see Eq. (2)]. Hence, combining Eqs. (15) with Eqs. (2) and (3) (and defining $d_0^{\mathrm{SD}} = d_0^T/f$), we obtain for the GL model

$$\omega\tau = \frac{\omega d^2}{6 d_0^{\mathrm{SD}} \exp(-q_0/kT)\exp(\mu_V T/k)} \quad . \tag{16}$$

Similarly, for the Seeger-Mehrer (SM) model $p_1(T)$ and $p_2(T)$ are governed by Eqs. (11a) and (11b), and the combination of Eqs. (15), (1), and (3) yields

$$\omega\tau = \frac{\omega d^2}{6 D_{01}^{\mathrm{SD}} \exp(-E_{1V}/kT)[1 + D_{21}\exp(-\epsilon E_{1V}/kT)]} \quad . \tag{17}$$

In the $T_{1\rho}$ case, in Eqs. (16) and (17), $\omega \equiv \omega_1$ while in the T_1 case, $\omega \equiv \omega_0$.

Using the theoretical values for the relaxation rates presented by Wolf[15] for mono- and divacancies as a function of the normalized jump time $\omega\tau$ together with Eqs. (10) and (11), the experimental $(T_{1\rho})_d$ data in Fig. 5 may be fitted in terms of both models. With the aid of a computer fit, the parameters in Eqs. (16) and (17), respectively, which minimize the mean-square deviation from the corresponding analytical expression were calculated. The values of the parameters thus obtained are listed in Table II. For comparison, the table also shows the corresponding parameters obtained from fits to the Arrhenius plot for the radio-tracer self-diffusion constant.[4,6]

The solid lines in Fig. 5 illustrate the quality of the computer fit of the experimental data with the sets of parameter values in Table II. Since the mean-square deviation is found to be about 5% for both models, the fit procedure leads to practically the same sets of curves in Fig. 5 associated with the two models.

Three different kinds of divacancy diffusion mechanisms[35] involving nearest-neighbor ($1N$), second- ($2N$), and fourth nearest-neighbor ($4N$) configurations of the two monovacancies forming a pair were assummed to interpret the NMR data by means of the SM model. In all three mechanisms the divacancy is assumed to migrate by nearest-neighbor jumps by either of its member monovacancies.[35] While from a $1N$ or a $4N$ configuration only jumps into a $2N$ configuration are thought to be possible,[35] the probabilities for jumps of the type $2N \rightarrow 1N$ and $2N \rightarrow 4N$ are governed by the temperature-dependent ratio ν_{24}/ν_{21} of the related jump frequencies. For example, in the $1N$-$2N$-$1N$ and the $2N$-$4N$-$2N$ mechanisms, ν_{24}/ν_{21} is assumed to equal zero and infinity, respectively.[35] To demonstrate a mechanism involving all three divacancy configurations, in the particular $1N$-$2N$-$4N$ mechanism considered we have chosen $\nu_{24}/\nu_{21} = 1$. It was found that the fits (and hence the Arrhenius plots discussed below) thus obtained differ even at the highest temperatures by less than 4% from the ones shown in Fig. 5 for the $1N$-$2N$-$1N$ mechanism. Furthermore, within the experimental error, a fit in terms of the $1N$-$2N$-$1N$ divacancy mechanism leads to the same set of parameters in Table II as a fit based on the $1N$-$2N$-$4N$ mechanism.

In principle, one might expect a motion-induced quadrupolar relaxation contribution to $(T_{1\rho})_d$ arising from the fluctuation of the electric field gradients associated with vacancies which interact with the quadrupole moment of neighboring Na nuclei.[33] Since the jump frequency $1/\tau_v$ of a vacancy is much larger (by

TABLE II. Parameters determining the curvature of the Arrhenius plot of sodium assuming the Seeger-Mehrer model [Eq. (1)] and the Gilder-Lazarus model [Eq. (2)], respectively.

	NMR	Tracer[a]
E_{1V}(eV)	0.372 ± 0.002	0.37 ± 0.01
E_{2V}(eV)	0.481 ± 0.002	0.50 ± 0.02
$D_{01}^{\mathrm{SD}}, D_{02}^T$ (cm^2 s^{-1})	$(4 \pm 1) \times 10^{-3}$	$(5.7 \pm 0.4) \times 10^{-3}$
$D_{02}^{\mathrm{SD}}, D_{02}^T$ (cm^2 s^{-1})	2.6 ± 0.3	0.72 ± 0.05
q_0(eV)	0.355 ± 0.005	0.338
d_0^{SD}, d_0^T (cm^2 s^{-1})	$(1.0 \pm 0.005) \times 10^{-4}$	1.12×10^{-4}
μ_v(eV K^{-2})	$(2.78 \pm 0.30) \times 10^{-6}$	

[a]See Refs. 4 and 6.

a factor $1/C_v$, where C_v is the vacancy concentration) than the jump frequency of a sodium atom, the $T_{1\rho}$ minimum associated with the quadrupolar relaxation contribution is expected for temperatures well below the minimum region in Fig. 1, namely, where $\omega_1\tau_v \simeq 1$.[33] But, as seen from Fig. 1, no deviation from the Korringa-like behavior of the relaxation time $T_{1\rho}$ was observed for temperatures below the minimum region. The reason for that is primarily due to the small vacancy concentration in the temperature range where $\omega_1\tau_v \approx 1$.

IV. SELF-DIFFUSION MECHANISM

The Arrhenius plots of D^{SD} for the SM model as well as for the GL model obtained with the parameter values in Table II are shown in Fig. 8 together with Mundy's radio-tracer data.[6] The correlation factors f obtained as the ratio D^T/D^{SD} [see Eq. (3)] from Fig. 8 are shown in Fig. 9. If monovacancies were the sole source of the curvature, the temperature-independent value $f = 0.727$ would have to be obtained when analyzing the NMR data in terms of this mechanism. Conversely, if divacancies would give rise to the curvature, the correlation factor thus obtained would have to be governed by the expression[3,19]

$$f = f_{1V} D_{1V}^{SD}/D^{SD} + f_{2V} D_{2V}^{SD}/D^{SD} \qquad (18)$$

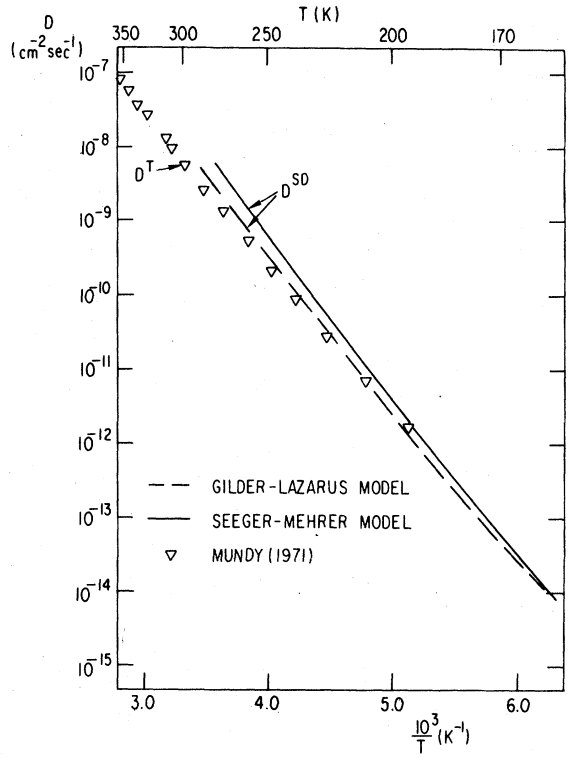

FIG. 8. Arrhenius plot of the self-diffusion coefficient D^{SD} in solid sodium evaluated from NMR measurements. Solid line: SM model. Dashed line: GL model. For comparison, Mundy's (Ref. 6) radio-tracer self-diffusion coefficients D^T (triangles) are also shown.

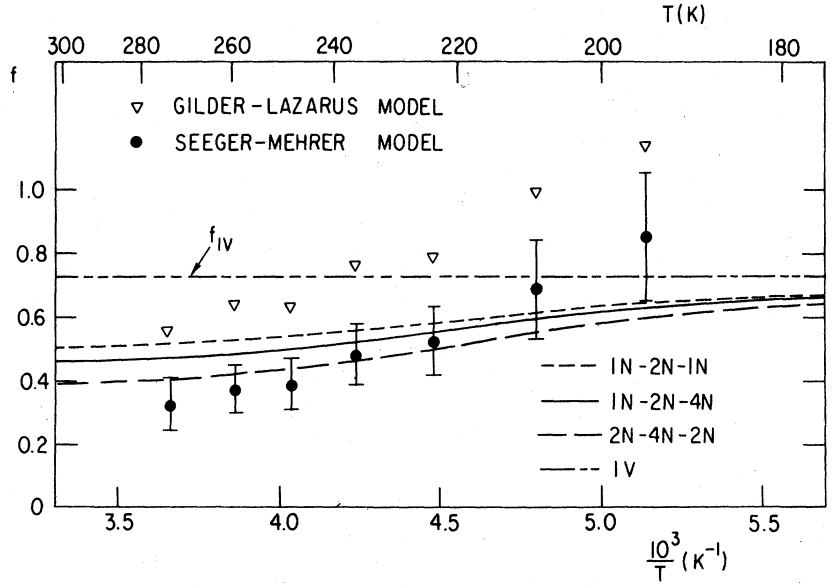

FIG. 9. Temperature dependence of the correlation factor $f = D^T/D^{SD}$ determined for the Seeger-Mehrer (SM) model (full circles) and Gilder-Lazarus (GL) model (triangles) from the results in Fig. 8. The curved lines represent the correlation factors calculated from Eq. (18) with the parameters listed in Table II for the three divacancy mechanisms considered. The error bars for the GL mechanism are identical with those for the SM mechanism.

in order for the NMR interpretation to be consistent with the radio-tracer measurements.

Figure 9 illustrates that the interpretation of the NMR data in terms of the GL model leads to a temperature-dependent correlation factor in contradiction to the assumption that monovacancies alone give rise to the curvature. Although the error bars are rather large, we believe that a straight line with $f=0.727$ does not fit the GL values as this would require a systematical experimental error, for example, in the temperature measurement. We have no reason to believe in the existence of any such systematical error.

The theoretical curves associated with divacancies in Fig. 9 were obtained from Eq. (18) using the values of D_{1V}^{SD} and D_{2V}^{SD} in Table II and the values $f_{2V}=0.43$ for the $1N$-$2N$-$4N$ mechanism, $f_{2V}=0.48$ for the $1N$-$2N$-$1N$ mechanism, and $f_{2V}=0.34$ for the $2N$-$4N$-$2N$ mechanism.[35] The agreement of the theoretical curves with the experimentally-determined f values is best for the $2N$-$4N$-$2N$ mechanism and poorest for the $1N$-$2N$-$1N$ mechanism if only one divacancy mechanism is operating. The data seems to require a $2N$-$4N$-$2N$ divacancy mechanism at higher temperatures while the other divacancy mechanisms may contribute significantly at lower temperatures. This suggests that the ratio ν_{24}/ν_{21} increases with increasing temperature.

Finally, let us consider the possibility that monovacancy double jumps give rise to the observed curvature in the Arrhenius plot. If about 10% of all monovacancy jumps are assumed to be double jumps[8] (as according to DaFano and Jaccucci[8] is appropriate for temperatures on the high-temperature side of the minimum region in Fig. 1), the correlation factor is found to increase from $f=0.727$ (for only nearest-neighbor jumps) to $f=0.739\pm0.006$. This value was determined from the computer simulation of the almost random vacancy motion using the Monte Carlo computer program of Wolf *et al.*[40] Similarly, for 25% double jumps we obtain $f=0.745\pm0.006$. The parameters entering into the NMR correlation functions which govern the theoretical relationship between the NMR relaxation time $(T_{1\rho})_d$ and τ were found to vary equally little with an increasing number of double jumps. Within a few percent, the Arrhenius plot (and hence the correlation factor) which one would obtain by interpreting our NMR results in terms of the DaFano-Jaccucci (FJ) model therefore agrees with the corresponding curves in Figs. 8 and 9 for the GL model.

As is obvious from Fig. 9, the corresponding values of f do not show the slight increase at higher temperatures necessary for the NMR results to be consistent with the tracer data for the FJ mechanism. In the temperature region investigated the FJ model does, therefore, not offer the correct answer as to the origin of the curvature in the Arrhenius plot of sodium.

V. CONCLUSIONS

Among the three diffusion models considered, only the combination of mono- and divacancies permits a self-consistent interpretation of the NMR and radiotracer results. In the temperature range investigated (150–280 K) the effects entering into the Gilder-Lazarus model and the DaFano-Jaccucci model involving monovacancies alone appear to play a minor role only. At higher temperatures the most likely mode of divacancy motion appears to favor $2N$ and $4N$ divacancy configurations over $1N$ configurations while at lower temperatures $1N$ configurations may play an important role in the diffusion process. As mentioned in the Introduction, our basic conclusions concerning the diffusion mechanism in sodium have been arrived at independently by Göltz *et al.*[24] by means of quasielastic neutron scattering.

It should be noted, however, that the temperature range in these experiments (323 K–melting point) does not overlap with the range accessible to NMR relaxation experiments.

ACKNOWLEDGMENTS

We would like to thank Dr. N. L. Peterson for many helpful discussions and his critical reading of the manuscript. We gratefully acknowledge Professor Van der Lugt's allowing the preparation of the samples in the glove box at the Metal Physics Laboratory of the University of Groningen, The Netherlands. The work was supported financially by the "Herbert-Quandt-Stiftung" and by the U.S. Department of Energy.

[1] A. Seeger and H. Mehrer, in *Vacancies and Interstitials in Metals,* edited by A. Seeger, D. Schumacher, W. Schilling, and J. Diehl (North-Holland, Amsterdam, 1970).
[2] H. Mehrer, Habilitationsschrift (Universität Stuttgart, 1973) (unpublished).
[3] H. Mehrer, J. Nucl. Mater. 69 and 70, 38 (1978).
[4] M. Gilder and D. Lazarus, Phys. Rev. B 11, 4916 (1975).
[5] P. Varatsos, W. Ludwig, and C. Falter, J. Phys. C 11, L311 (1978).
[6] J. N. Mundy, Phys. Rev. B 3, 2431 (1971).
[7] C. H. Bennett, in *Proceedings of the 19th ême Colloque du Metallurgie, Saclay, 1976* (Centre d'Etudes Nucleaires de Saclay, Saclay, 1976), Vol. II, p. 65.
[8] A. DaFano and G. Jaccucci, Phys. Rev. Lett. 39, 950 (1977).

[9]J. N. Mundy, L. W. Barr, and F. A. Smith, Philos. Mag. 14, 785 (1966).
[10]R. Feder and H. P. Charbnau, Phys. Rev. 149, 464 (1966).
[11]W. Adlhart, G. Fritsch, and E. Lüscher, J. Phys. Chem. Solids 36, 1405 (1975).
[12]N. L. Peterson, Comments Solid State Phys. 8, 107 (1978).
[13]D. Wolf, Phys. Rev. B 10, 2710 (1974).
[14]D. Wolf, Phys. Rev. B 10, 2724 (1974).
[15]D. Wolf, Phys. Rev. B 15, 37 (1977).
[16]D. Wolf, Solid State Commun. 23, 853 (1977).
[17]D. Wolf, Appl. Phys. Lett. 30, 617 (1977).
[18]D. Wolf, J. Nucl. Mater. 69 and 70, 536 (1978).
[19]D. Wolf, J. Appl. Phys. 49, 2752 (1978).
[20]R. Messer, Ph.D thesis (Universität Stuttgart, 1976) (unpublished).
[21]See also Mehrer's report on Messer's results in Ref. 3.
[22]A. Lodding, J. N. Mundy, and A. Ott, Phys. Status Solidi 38, 559 (1970).
[23]M. Ait-Salem, T. Springer, A. Heidemann, and B. Alefeld, Philos. Mag. B 39, 797 (1979).
[24]G. Göltz, A. Heidemann, H. Mehrer, A. Seeger, and D. Wolf, Philos. Mag. A 41, 723 (1980).
[25]D. F. Holcomb and R. E. Norberg, Phys. Rev. 98, 1074 (1955).
[26]R. A. Hultsch and R. G. Barnes, Phys. Rev. 125, 1832 (1962).
[27]J. Jeener and P. Broeckaert, Phys. Rev. 157, 232 (1967).
[28]B. R. McGarvey and H. S. Gutowsky, J. Chem. Phys. 21, 2114 (1953).
[29]C. P. Slichter, *Principles of Magnetic Resonance* (Harper and Row, New York, 1963); L. C. Hebel and C. P. Slichter, Phys. Rev. 113, 1504 (1959).
[30]G. B. Benedek and T. Kushida, J. Phys. Chem. Solids 5, 241 (1958).
[31]*Landolt-Bornstein* (Springer, Berlin, 1971), Vol. II, Part 1.
[32]L. E. Drain, Metall. Rev. 12, 195 (1967).
[33]D. Wolf, *Spin Temperature and Nuclear Spin Relaxation in Matter* (Clarendon, Oxford, 1979).
[34]M. Goldmann, *Spin Temperature and Nuclear Magnetic Resonance in Solids* (Clarendon, Oxford, 1970).
[35]H. Mehrer, J. Phys. F 3, 543 (1973).
[36]Please note the error in the definition of p_1 in Eqs. (2.12) and (2.25) of Ref. 15. Rather than defining p_1 via the relative number of *jumps* of mono- and divacancies, p_1 should be properly defined as the ratio of the related *diffusion coefficients*, i.e., $p_1 = D_1/(D_1 + D_2)$. This leads to a slight modification of the expressions (2.26) to (2.28) in Ref. 15. We are grateful for discussions with K. Schroeder on this subject.
[37]C. P. Slichter and D. C. Ailion, Phys. Rev. 137, A235 (1965).
[38]D. C. Ailion and P. P. Ho, Phys. Rev. 168, 662 (1968).
[39]J. R. Franz and R. Gujral, Phys. Rev. B 8, 5321 (1973).
[40]D. Wolf, K. Differt, and H. Mehrer, Comput. Phys. Commun. 13, 183 (1977).